Bacteriophage anti-defense genes that neutralize TIR and STING immune responses

Peiyin Ho[1], Yibu Chen[2], Subarna Biswas[3], Ethan Canfield[4] and Douglas E. Feldman[1,5*]

[1]Department of Pathology

[2]Bioinformatics Service, Department of Health Sciences Libraries

[3]Department of Surgery

University of Southern California, Keck School of Medicine, Los Angeles, CA 90033, USA

[4]University of Southern California, School of Pharmacy, Los Angeles, CA 90033, USA

[5]Lead contact

*Correspondence: defeldma@usc.edu

Summary

Programmed cell suicide of infected bacteria, known as abortive infection (Abi), serves as a central immune defense strategy to prevent the spread of bacteriophage viruses and other invasive genetic elements across a population. Many Abi systems utilize bespoke cyclic nucleotide immune messengers generated upon infection to rapidly mobilize cognate death effectors. Here, we identify a large family of bacteriophage nucleotidyltransferases (NTases) that synthesize competitor cyclic dinucleotide (CDN) ligands, inhibiting NAD-depleting TIR effectors activated by a STING CDN sensor domain. Virus NTase genes are positioned within genomic regions containing other anti-defense genes, and through a functional screen, we uncover candidate anti-cell suicide (Acs) genes that confer protection against TIR-STING cytotoxicity. We show that a virus MazG-like pyrophosphatase identified in the screen, Acs1, depletes the starvation alarmone (p)ppGpp, impairing activation of the MazF suicide toxin. Phage NTases and counter-defenses like Acs1 preserve host viability to ensure virus propagation, and may be exploited as tools to modulate TIR and STING immune responses.

Introduction

Bacteria are under the constant threat of attack from viruses (phages) and other mobile genetic elements (MGE), and have evolved a multitude of defenses, ranging from restriction enzymes to CRISPR/Cas adaptive immunity, to mitigate this threat. Programmed bacterial cell suicide, known as abortive infection (Abi), represents a primary strategy employed by infected cells to block the colony-wide propagation of viruses and achieve population-level immunity, at the expense of individual survival (1, 2).

Early studies on operon-linked toxin-antitoxin (TA) systems, as well as more recent discoveries on retrons, have revealed the regulatory logic underlying Abi immune responses. In contrast to restriction enzymes and CRISPR/Cas, which are tonically active but narrowly targeted to specific sequences in foreign, but not host, nucleic acids (3-5), highly cytotoxic Abi systems must first be activated by sensing intrusion of the MGE into the cell. TA systems are armed through a combination of a labile antitoxin and the convergence of multiple stressors, such as phage infection, that downregulate transcription of the TA operon, resulting in rapid loss of the antitoxin and activation of a lethal toxin (6, 7). Retrons are likewise held in an inactive state until their toxicity is unleashed through engagement with specific phage proteins (8).

Nucleotide-based immune alarm signaling has emerged as a central mechanism across distinct Abi systems. Type III CRISPR-Cas, Pycsar, and cyclic dinucleotide-based antiphage signaling systems (CBASS) are triggered through activation of constituent nucleotidyltransferases (NTases) and nucleotide cyclases upon phage infection (9-11). Cyclic nucleotide messengers generated by these enzymes mobilize cognate death effectors, including nucleases, proteases, pore-forming toxins, as well as sirtuin and Toll-interleukin-1 receptor (TIR) domain NAD-cleaving enzymes (11-13), through direct binding to an effector-linked cyclic nucleotide sensor, such as the widespread STING (stimulator of interferon genes) domain. Many viruses, in turn, deploy specialized nucleases that rapidly cleave and inactivate cyclic nucleotides, extinguishing host immune responses (14, 15).

Currently, our understanding of how viruses evade the multitude of known Abi systems is limited, and little is known about whether viruses employ counter-defense strategies beyond signal degradation. This stands in contrast to the large repertoire of experimentally characterized anti-CRISPRs, many of which inactivate CRISPR/Cas subtypes with exquisite specificity (16, 17). Here, we uncover a family of virus-encoded NTases that generate CDN competitor ligands that impair activation of TIR death effectors containing a linked STING CDN

sensor domain (TIR-STING). We show that virus genes encoding NTases are positioned in close proximity to known anti-defense genes, and through a plasmid-based functional screen, we identify novel virus anti-cell suicide (Acs) candidate genes. Among these, we uncover a phage MazG-like enzyme, Acs1, that depletes the starvation alarmones (p)ppGpp, revealing how TIR-mediated abortive infection is executed, in part, through alarmone-activated host toxins.

Results

Bioinformatic analysis of bacteriophage genomes across the *Siphoviridae*, *Myoviridae* and *Podoviridae* virus families revealed a large group of genes encoding predicted NTases that are closely related to the minimal NTases (MNT) of the polβ NTase superfamily (4), with a more distant relationship to kanamycin NTases (KNT) (Figure 1A). While phage NTases contain an intact catalytic site GS-x-AY[GAN]T-x4-SDxD that is similar to that found in MNT, they lack a near-invariant tyrosine (Y) residue that is positioned immediately C-terminal to the GS motif in MNT (Figure 1B, site 1). Furthermore, phage NTases, but not MNT, contain a conserved NP-x-h2[DE] sequence positioned approximately 60 residues C-terminal to the SDxD motif (Fig, 1B, site 2). This sequence divergence supports the proposal that phage NTases encompass a distinct clade within the NTase superfamily.

To examine possible enzymatic functions of phage NTases, we incubated purified, recombinant NTases from the *Bacillus* phage BCP1 and Enterobacteriophage Av05 in the presence of rNTPs. Wild-type BCP1 NTase, but not a catalytic site mutant (SDWD→AAWA), generated 3’3’cGAMP and cyclic di-adenylate (cAA) as major products, as determined by MALDI-MS profiling (Figures 1C, S1A and S1B). Av05 NTase likewise generated 3’3cGAMP and cAA, as well as a product consistent with the mass of cyclic uridine-adenylate (cUA) (Figures 1D and S1C). These findings expand the range of NTase families that are capable of synthesizing CDN products.

While 3’3’cGAMP acts as an immune alarm signal that mobilizes host CBASS death effectors (9, 13, 18), the widespread distribution of NTases across virus families suggests that phage CDN synthesis may confer a fitness advantage. In line with this proposal, 3’3’cGAMP binds, with varying affinities, to STING CDN sensor domains contained within TIR-STING effectors from different species, and can act as a competitive inhibitor of the activating ligand cyclic di-guanylate (cGG) (19). We therefore sought to explore the effect of phage NTases on TIR-STING, using cleavage of the fluorogenic substrate ε-NAD as a measure of enzymatic activity.

Co-incubation of *S. falciparum* (*Sf*) TIR-STING with cGG and increasing amounts of BCP1 and Av05 NTases resulted in a concentration-dependent inhibition of the initial ε-NAD cleavage rate, while a BCP1 catalytic mutant had no effect on TIR-STING NADase activity (Figure 2A). When introduced into *E. coli*, BCP1 and Av05 phage NTases protected hosts against the toxic effects of *Sf*TIR-STING, as determined through colony forming unit (CFU) assays, while the BCP1 catalytic mutant failed to do so (Figure 2B). In contrast, BCP1 NTase was largely ineffective in inhibiting the enzymatic activity of *Capnocytophage granulosa* (*Cg*) TIR-STING, which exhibits a 100-fold lower affinity for 3'3'cGAMP relative to that of *Sf*STIR-STING (19) (Figure S2A), and did not protect hosts against *Cg*TIR-STING (Figure S2B). Collectively, these results suggest that phage NTases generate competitor CDN ligands such as 3'3'cGAMP as a strategy to inhibit TIR-STING immune effectors.

Phage anti-restriction and anti-CRISPR genes are often positioned together within larger anti-defense gene clusters (16, 20). We therefore performed a bioinformatics analysis of genes flanking phage NTases. Starting from a set of 240 phage NTases (Table S1), we identified 1958 flanking open reading frames (ORFs), encompassing 332 clusters of closely related sequences. Among these, we found DNA adenine and cytosine methyltransferases, which block host restriction endonucleases, and NAD+ biosynthetic enzymes that may mitigate the metabolite-depleting effects of TIR NADases (Figure 3A). This suggested that previously unrecognized anti-defense genes may be positioned in close proximity to genes encoding NTases.

To identify additional candidate anti-defense genes, we performed a plasmid-based functional screen for phage ORFs that are selectively enriched when co-expressed with a TIR-STING death effector, but not in the presence of an empty vector control. We first co-transformed *E. coli* with an inducible plasmid library encompassing 257 NTase-adjacent ORFs (size cutoff, 200 amino acids), representative of 176 sequence clusters, together with a second inducible plasmid encoding TIR-STING or an empty vector control. Each transformant strain was then inoculated into liquid culture, and subsequently shifted to growth under inducing conditions before cell recovery (Figure 3B). We PCR amplified the phage insert region of the input plasmid library and the output plasmid library following overnight growth under inducing conditions, and used next-generation sequencing to compare the representation of individual inserts in the input and output plasmid libraries.

Following this approach, we identified six phage genes that are significantly enriched (FC>2, P<0.05) in bacterial hosts co-expressing TIR-STING, but an empty control plasmid, suggesting that these genes confer protection against TIR-STING toxicity and provide a survival advantage

(Figure 3C). While most ORFs showed no detectable sequence similarity to any previously characterized protein, a gene from Pectobacterium phage PcCB7V encoding a MazG-like protein was significantly enriched in the screen (Figures 3C and 3D). In *E. coli,* the *mazG* gene is positioned downstream of *relA* within the *mazEF* TA operon, a stress-induced cell suicide module. MazF is a stable endoribonuclease toxin that is inhibited through a direct interaction with its cognate antitoxin MazE, a labile protein (21). Under conditions of nutrient deprivation, RelA senses deacylated tRNA in the ribosomal A-site of starved ribosomes, and synthesizes the alarmone nucleotides guanosine pentaphosphate (pppGpp) and tetraphosphate (ppGpp)—collectively referred to as (p)ppGpp—that globally downregulate transcription as part of the stringent response, resulting in rapid loss of the MazE antitoxin and activation of the promiscuous MazF endoribonuclease toxin (22, 23).

The identification of a phage MazG-like protein, which we have provisionally designated Acs1 (*a*nti-*c*ell *s*uicide 1), as a hit in the screen suggested that enzymatic depletion of (p)ppGpp may attenuate TIR-mediated cell suicide. Consistent with this possibility, purified wild-type Acs1 stimulated the dephosphorylation of ppGpp substrate with an apparent Km of ~50 μM (Figures 3E and S3A), a value that is above intracellular concentrations of (p)ppGpp during logarithmic growth but would allow for maximal enzyme activity following induction of the stringent response (24, 25). In contrast, no significant effect of Acs1 was seen on dephosphorylation of rNTPs or cGG under the same reaction conditions (Figures 3E and S3B).

We next utilized an RNA-based fluorescent (p)ppGpp sensor (26) to monitor the effects of TIR-STING expression on cellular alarmone pools. Live-cell imaging revealed significant fluorescence activation following induction of TIR-STING (Figure 4A), with a mean 2.7-fold increase in signal intensity relative to glucose-fed control cells, similar to the increase seen in cells exposed to a chemical inducer of starvation, α-methylglucose (α-MG) (Figures 4A and 4B). Conversely, phage MazG suppressed reporter fluorescence following 1 h exposure to α-MG (Figures 4C and 4D). Taken together, these observations indicate that TIR-STING triggers a rapid increase in cellular (p)ppGpp pools, and that this response can be suppressed by Acs1.

To assess the contribution of (p)ppGpp and the stringent response to TIR-STING toxicity, we performed CFU assays to measure and compare the viability of *mazG, relA* and *mazEF* mutants expressing TIR-STING, relative to wild-type parental control strains. Loss of *mazG*, which confers hypersensitivity to amino acid starvation (21), led to a 4-fold further decrease in viability upon TIR-STING expression, relative to a parental strain (Figures 5A and 5B). Conversely, mutational inactivation of *relA* or *mazEF* protected cell viability from TIR-STING toxicity (Figures

5A and 5B). Bacteriophage lambda RexB, which inhibits the proteolytic degradation of MazE to maintain the MazF toxin in an inactive conformation (27), also increased the viability of cells co-expressing TIR-STING, as did Acs1, validating the results from the primary screen (Figure 5A and B).

Notably, Acs1 also blunted the toxic effects of a distinct TIR domain death effector, retron-TIR (28), partially rescuing plaque formation by the T5 bacteriophage, relative to a control strain that did not express Acs1 (Figure 5C). These observations together indicate that Acs1 can confer protection against distinct defense systems that utilize TIR domain-containing effectors (Figure 5D).

Discussion

Abortive infection is an immune strategy predicated on host self-destruction that is designed to rapidly extinguish the spread of viruses and other invasive genetic elements across a bacterial population, at the expense of individual cell survival. Here, we uncover virus anti-defense genes that counteract cytotoxic Abi effectors containing the widespread and highly conserved TIR and STING domains. These anti-Abi systems operate through distinct, nucleotide-centered mechanisms: the production of competitive inhibitor CDNs that can “jam” STING receptors, and the enzymatic depletion of (p)ppGpp alarmone molecules, impairing the host response to metabolite depletion by NAD-hydrolyzing TIR enzymes and the ensuing mobilization of cytotoxins.

We identify a large family of virus-encoded NTases that synthesize cAA and 3’3’cGAMP as major products, the same CDNs that act as immune messengers generated by bacterial CD-NTases encoded within host CBASS defense systems (9). Virus NTases are closely related to bacterial and archaeal MNT within the polβ-type NTase superfamily, while exhibiting a more distant sequence relationship to kanamycin NTases, which confer resistance to aminoglycoside antibiotics (29). These observations expand the scope of NTase families known to synthesize CDNs, and suggest that bacterial MNT enzymes may likewise generate CDN products. In contrast to CD-NTases and nucleotide cyclases contained, respectively, within CBASS and Pycsar systems (9, 10, 18), phage NTase are not encoded within operons containing known cyclic nucleotide sensor or effector domains. Rather, by generating 3’3’cGAMP, virus NTases may competitively inhibit host STING receptors, many of which can bind to distinct CDNs but are selectively activated by cGG (19). It will be important to determine whether this signal jamming strategy extends beyond TIR-STING to other classes of

nucleotide-sensing effectors, such as those containing the widespread SAVED, patatin and SLOG domains (12, 13, 30).

Our results additionally reveal the general design for a second virus anti-suicide system that exploits a previously unrecognized dependency of TIR NADase-driven cell death on production of the stringent response alarmones (p)ppGpp. We show that a virus MazG-like protein, Acs1, depletes cellular (p)ppGpp pools, blocking the mobilization of host TA suicide modules, including MazEF. Thus, while depletion of the essential metabolites NAD+ and NADP is thought to induce metabolic arrest (19), the combinatorial engagement of secondary death pathways may be required for maximal toxicity of TIR effectors. The transmission of cytotoxic signals downstream of TIR may occur not only through the activation of host metabolic stress pathways, as shown here, but additionally through the generation of the NAD cleavage product cyclic ADP ribose (cADPR), which itself can act as a messenger that mobilizes downstream immune effectors (12, 31, 32).

The identification of anti-Abi gene neighborhoods within phage genomes opens avenues for the systematic screening and identification of new classes of immune modulators. The diversity of bacterial Abi defenses, and the conservation and modularity of key effector domains such as TIR and STING (12, 28), highlights the potential for anti-Abi systems in the engineered control of immune signaling and cell survival.

Methods

Evolutionary and LOGO sequence analysis of NTase enzymes

Bacteriophage genes within the *Siphoviridae*, *Myoviridae* and *Podoviridae* families annotated as nucelotidyltransferases and containing intact catalytic motifs were used as query sequences for iterative BLAST searches. Evolutionary analyses were conducted with MEGA software (33) using the Maximum Likelihood method and JTT matrix-based model (34). The tree with the highest log likelihood is shown. Initial trees for the heuristic search were obtained automatically by applying Neighbor-Join and BioNJ algorithms to a matrix of pairwise distances estimated using the JTT model, and then selecting the topology with superior log likelihood value. Trees were visualized using iTOL v6. The tree is drawn to scale, with branch lengths measured in the number of substitutions per site. LOGO sequence analysis of NTase catalytic domains was performed using WebLogo (35).

Recombinant protein expression and purification

Synthetic gene fragments (gBlocks, IDT) encoding BCP1 and Av05 phage NTases, *Sf* and *Cg* TIR-STING, and Acs1 and containing an N-terminal TEV cleavage site were cloned directly via Gibson assembly (NEBuilder HiFi, New England Biolabs) into BamHI/NotI-digested pGEX4-1 (GE Healthcare), or tagged with N-terminal TwinStrep (TS) or streptavidin binding peptide (SBP) tags by PCR and introduced into NdeI/XhoI-digested pET30a vector (MilliporeSigma). Mutagenesis was performed using the Q5 Site-Directed Mutagenesis kit (New England Biolab). All constructs were confirmed by Sanger sequencing on both strands. Plasmids were transformed into BL21 (DE3) Rosetta 2 competent cells (MilliporeSigma). Bacterial cultures were grown to an A_{600} of 0.4-0.5, then induced with 0.1 mM IPTG for 16 hours at 30°C. Bacterial pellets were resuspended in ice-cold PBS supplemented with complete protease inhibitor cocktail, 5 mM sodium fluoride, 1 mM sodium orthovanadate, lysozyme (0.2 mg/ml) and DNase I (10 μg/ml), then sonicated in 5-6 bursts of 15 s with 30 s cooling in between bursts. Soluble proteins (5 ml) were incubated with 250 μl magnetic glutathione resin (ThermoFisher) or streptactin resin (IBA Life Sciences) for 2 h at 4°C with gentle rotation. Resin was washed three times in lysis buffer and eluted twice for 30 min in elution buffer (50 mM Tris-HCl pH 8.0, 200 mM NaCl, 5% glycerol, 10 mM desthiobiotin or glutathione), then pooled and dialyzed overnight at 4°C into TBS containing 5% glycerol. Samples were aliquoted and stored at -80°C.

Nucleotide synthesis assays

In vitro biochemical reactions were performed with 1 uM purified enzyme in NTase reaction buffer (50 mM Tris pH 8.0, 50 mM KCl, 5 mM $Mg(OAc)_2$, 1 mM DTT, 5% glycerol, 125 µM rNTPs) in a final volume of 20 µl for 3 h at 37°C. Reactions were deproteinized for MALDI-MS analysis with 80 µl acetonitrile and stored at -20°C prior to analysis.

MALDI-MS analysis

Samples were desalted and concentrated using ZipTip C18 micropipette tips (MilliporeSigma), then spotted on a 96-spot steel plate target and covered with alpha-cyano-4-hydroxy-cinnamic acid (HCCA) matrix solution. Mass spectrometry analysis was performed with a Microflex MALDI-TOF mass spectrometer (Bruker Daltonics) and spectra were recorded for positive ions. Polytools (2.0) software was used to analyze mass spectra.

TIR NADase assay

In vitro TIR NADase assays were performed essentially as described. Briefly, purified TIR-STING (0.5 µM) was incubated in TIR reaction buffer (20 mM HEPES-KOH pH 7.5, 100 mM KCl) containing 0.25 mM ε-NAD substrate and supplemented with 125 µM rNTPs, in the absence or presence of increasing amounts of purified Av05 NTase or the wild-type or mutant forms of BCP1 NTase 0.125, 0.25,1.25 µM). Reactions were performed in 96-well plates and initiated through the addition of cGG (40 nM), and read continuously using Synergy H1 Hybrid Multi-Mode Reader (BioTek) in fluorescence mode at 410 nm with excitation at 300 nm. Initial reaction rates are calculated using values obtained immediately prior to cGG addition, and at the 10 min time point.

Bacterial CFU assays

relA and *mazG* mutant and wild-type parental *E. coli* strains were obtained from the Keio Strain Collection (Horizon Discovery). The *mazEF* mutant and parental strains were a generous gift from Dr. Hanna Engelberg-Kulka. Cells from overnight cultures were diluted 1:20 in 5 ml of M9 medium containing 0.25% casamino acids (CAA) and 0.5% glucose. Cultures were grown with shaking at 200 rpm at 37°C to early log phase (OD_{600} 0.2-0.3). Cells were then washed in M9 minimal medium, serially diluted, and plated on M9 agar plates containing 0.25% CAA and 0.25% glucose; or 1% glycerol, 0.7% arabinose, as well as 0.5 mM IPTG for pET vector induction. Plates were incubated at 37°C overnight, and cell survival was evaluated by

comparing the colony-forming ability of cells under inducing and nutrient limiting conditions, normalized to the total number of viable cells grown on plates containing glucose.

Computational analysis of phage NTase-adjacent ORFs

Phage NTases were compiled at NCBI Protein and aligned using Jalview (36) to confirm the presence of intact catalytic motifs (GS and DXD). Protein-coding ORFs positioned within 4 genes of phage NTases were identified using webFlaGs (37) and their corresponding protein sequences downloaded using NCBI Batch Entrez. To reduce redundancy, highly similar sequences (at least 98% sequence identity and coverage) were discarded using the linclust option in MMseqs2 (38, 39) with parameters --min-seq-id 0.98 -c 0.98, and the resulting sequences clustered based on homology using the cascaded clustering option in MMSeqs2 to yield a list of 1603 ORFs distributed across 332 clusters. Uncharacterized ORFs less than 200 amino acids (257 ORFs representative of 176 clusters) were selected for functional screening studies.

Phage ORF library screening

Double-stranded gene fragments and pooled, single-stranded DNA oligonucleotides encoding phage ORFs with 20-25 nt flanking regions of homology to the pET-SUMO2 vector flanking the NdeI and NotI sites were purchased from IDT (eBlocks and oPools). ssDNA oligos were converted to dsDNA through isotheral extension of a primer complementary to the 3' flanking region (sparQ HiFi PCR Master Mix, Quantabio), and products purified with a DNA spin column. Pooled ORFs were inserted into pET-SUMO2 by DNA assembly (NEBuilder HiFi) and transformed into *E. coli* (NEB DH5α). Colonies were scraped from plates, combined and inoculated into 10 ml liquid cultures. Plasmid DNA encoding the pooled ORF library was then prepared and used to transform BL21 (DE3) Rosetta 2 competent cells (MilliporeSigma) together with pET30a encoding Flag-TIR-STING or empty vector control. 100 µl of overnight cultures were diluted 1:20 and grown in M9 media supplemented with 0.25% CAA and 1% glycerol, and induced at A_{600}=0.3-0.4 through the addition of 0.5mM IPTG. Samples were taken immediately prior to induction and at 18 h post-induction. Plasmid DNA was recovered by miniprep, and library inserts amplified by PCR using primers flanking the ORF insertion site in pET-SUMO2. Bar-coded libraries for Illumina sequencing were generated using the sparQ DNA Library Kit (Quantabio) and 50 bp reads generated using a HiSeq3000 sequencing system.

Pyrophosphatase assay

Phosphatase reactions were performed in 96-well plates in pyrophosphatase reaction buffer (50 mM Tris-HCl (pH 7.5), 250 mM KCl, 5 mM MgCl2, 1 mM TCEP) containing 1 µg of purified Acs1 protein and ppGpp, NTPs, or cGG for 1.5 h at 37°C. Reactions were stopped through addition of 10 µl of ice-cold 20 mM EDTA. Phosphate levels in each reaction were measured using the PiPer Pyrophosphate Assay Kit (ThermoFisher) following the manufacturer's instructions. Absorbance values determined using a Synergy H1 Hybrid Plate Reader set for absorbance at 565 nm.

Live cell imaging

E. coli BL21(DE3) cells carrying the S2 fluorescent sensor plasmid (26) were grown in M9 medium supplemented with 0.25% CAA and 0.5% glucose to an A_{600} of 0.2-0.4. Cells were briefly pelleted (8,000 x g, 45 s), then shifted to M9 medium containing 0.25% CAA, 0.5% glucose and 0.5mM IPTG, in the absence or presence of 2.5% α-MG to induce chemical starvation; or M9 containing 1% glycerol, 0.5mM IPTG and 0.75% arabinose to induce both nutrient deprivation and expression of TIR-STING from the pBAD vector. Cells were incubated with DFHBI-1T dye 1 h after shift to inducing media as described (26). Images were obtained using a Zeiss LSM 880 Airyscan confocal microscope and were quantified using ImageJ (1.53r) software.

Phage plaque assay

Bacterial overnight cultures grown from a single colony of *E. coli* K-12 strain MG1655 that had been transformed with retron-TIR from *Shigella dysenteriae* NCTC2966 (Addgene #157883) or an empty vector control (pACYC184) were grown in LB media, and a 1:100 dilution grown in a shaker at 37ºC at 200 rpm until the A_{600} reached 0.4-0.5. Next, 3 ml pre-warmed top agar (M9 salts, 0.25% CAA, 1% glycerol, 0.75% agar) was mixed with 0.15 ml bacteria culture, and poured evenly onto agar plates containing 25 ug/ml chloramphenicol . T5 phage (ATCC 11303-B5) was propagated by the double agar overlay method, and plaques scraped into LB media. Phage samples were centrifuged to pellet cellular debris, and the supernatant was filtered through with a 0.22 µm sterile filter. Phage preparations were serially diluted in phage dilution buffer (20 mM Tris pH 8.0, 150 mM NaCl, 8 mM $MgS0_4$) and 4 µl droplets of each dilution spotted onto the cooled top agar layer. Plaques were allowed to form for 16 h at 37°C.

Acknowledgements

This project is supported in part by grant 5R21AA027535-02 from the NIH, IRG-16-181-57 from the American Cancer Society, and the USC Department of Pathology. We thank Dr. Alireza Abdolvahabi for assistance with MALDI-MS experiments and Dr. Aaron Whiteley for helpful discussions. We have no conflicts of interest to disclose.

Author Contributions

P.H. performed biochemical assays and experiments with bacterial cells, and prepared libraries for next-generation sequencing. E.C. directed mass spectrometry analysis. Y.C. and S.B. performed bioinformatics analysis. P.H., and D.E.F. analyzed the data and wrote the manuscript.

Declaration of Interests

The authors declare no competing interests.

References

1. Lopatina A, Tal N, Sorek R. Abortive Infection: Bacterial Suicide as an Antiviral Immune Strategy. Annu Rev Virol. 2020;7(1):371-84. Epub 20200619. doi: 10.1146/annurev-virology-011620-040628. PubMed PMID: 32559405.
2. Chopin MC, Chopin A, Bidnenko E. Phage abortive infection in lactococci: variations on a theme. Curr Opin Microbiol. 2005;8(4):473-9. doi: 10.1016/j.mib.2005.06.006. PubMed PMID: 15979388.
3. Jinek M, Chylinski K, Fonfara I, Hauer M, Doudna JA, Charpentier E. A programmable dual-RNA-guided DNA endonuclease in adaptive bacterial immunity. Science. 2012;337(6096):816-21. Epub 20120628. doi: 10.1126/science.1225829. PubMed PMID: 22745249; PubMed Central PMCID: PMC6286148.
4. Haurwitz RE, Jinek M, Wiedenheft B, Zhou K, Doudna JA. Sequence- and structure-specific RNA processing by a CRISPR endonuclease. Science. 2010;329(5997):1355-8. doi: 10.1126/science.1192272. PubMed PMID: 20829488; PubMed Central PMCID: PMC3133607.
5. Pingoud A, Fuxreiter M, Pingoud V, Wende W. Type II restriction endonucleases: structure and mechanism. Cell Mol Life Sci. 2005;62(6):685-707. doi: 10.1007/s00018-004-4513-1. PubMed PMID: 15770420.
6. Jurėnas D, Fraikin N, Goormaghtigh F, Van Melderen L. Biology and evolution of bacterial toxin-antitoxin systems. Nat Rev Microbiol. 2022;20(6):335-50. Epub 20220102. doi: 10.1038/s41579-021-00661-1. PubMed PMID: 34975154.
7. Harms A, Brodersen DE, Mitarai N, Gerdes K. Toxins, Targets, and Triggers: An Overview of Toxin-Antitoxin Biology. Mol Cell. 2018;70(5):768-84. Epub 20180203. doi: 10.1016/j.molcel.2018.01.003. PubMed PMID: 29398446.
8. Millman A, Bernheim A, Stokar-Avihail A, Fedorenko T, Voichek M, Leavitt A, et al. Bacterial Retrons Function In Anti-Phage Defense. Cell. 2020;183(6):1551-61.e12. Epub 20201105. doi: 10.1016/j.cell.2020.09.065. PubMed PMID: 33157039.
9. Whiteley AT, Eaglesham JB, de Oliveira Mann CC, Morehouse BR, Lowey B, Nieminen EA, et al. Bacterial cGAS-like enzymes synthesize diverse nucleotide signals. Nature. 2019;567(7747):194-9. Epub 2019/02/20. doi: 10.1038/s41586-019-0953-5. PubMed PMID: 30787435; PubMed Central PMCID: PMC6544370.
10. Tal N, Morehouse BR, Millman A, Stokar-Avihail A, Avraham C, Fedorenko T, et al. Cyclic CMP and cyclic UMP mediate bacterial immunity against phages. Cell. 2021;184(23):5728-39.e16. Epub 20211012. doi: 10.1016/j.cell.2021.09.031. PubMed PMID: 34644530; PubMed Central PMCID: PMC9070634.

11. Kazlauskiene M, Kostiuk G, Venclovas Č, Tamulaitis G, Siksnys V. A cyclic oligonucleotide signaling pathway in type III CRISPR-Cas systems. Science. 2017;357(6351):605-9. Epub 20170629. doi: 10.1126/science.aao0100. PubMed PMID: 28663439.
12. Ofir G, Herbst E, Baroz M, Cohen D, Millman A, Doron S, et al. Antiviral activity of bacterial TIR domains via immune signalling molecules. Nature. 2021;600(7887):116-20. Epub 20211201. doi: 10.1038/s41586-021-04098-7. PubMed PMID: 34853457.
13. Lowey B, Whiteley AT, Keszei AFA, Morehouse BR, Mathews IT, Antine SP, et al. CBASS Immunity Uses CARF-Related Effectors to Sense 3'-5'- and 2'-5'-Linked Cyclic Oligonucleotide Signals and Protect Bacteria from Phage Infection. Cell. 2020;182(1):38-49.e17. Epub 20200615. doi: 10.1016/j.cell.2020.05.019. PubMed PMID: 32544385; PubMed Central PMCID: PMC7728545.
14. Hobbs SJ, Wein T, Lu A, Morehouse BR, Schnabel J, Leavitt A, et al. Phage anti-CBASS and anti-Pycsar nucleases subvert bacterial immunity. Nature. 2022;605(7910):522-6. Epub 20220408. doi: 10.1038/s41586-022-04716-y. PubMed PMID: 35395152.
15. Athukoralage JS, McMahon SA, Zhang C, Grüschow S, Graham S, Krupovic M, et al. An anti-CRISPR viral ring nuclease subverts type III CRISPR immunity. Nature. 2020;577(7791):572-5. Epub 20200115. doi: 10.1038/s41586-019-1909-5. PubMed PMID: 31942067; PubMed Central PMCID: PMC6986909.
16. Marino ND, Zhang JY, Borges AL, Sousa AA, Leon LM, Rauch BJ, et al. Discovery of widespread type I and type V CRISPR-Cas inhibitors. Science. 2018;362(6411):240-2. Epub 20180906. doi: 10.1126/science.aau5174. PubMed PMID: 30190308; PubMed Central PMCID: PMC6520112.
17. Bondy-Denomy J, Garcia B, Strum S, Du M, Rollins MF, Hidalgo-Reyes Y, et al. Multiple mechanisms for CRISPR-Cas inhibition by anti-CRISPR proteins. Nature. 2015;526(7571):136-9. Epub 20150923. doi: 10.1038/nature15254. PubMed PMID: 26416740; PubMed Central PMCID: PMC4935067.
18. Cohen D, Melamed S, Millman A, Shulman G, Oppenheimer-Shaanan Y, Kacen A, et al. Cyclic GMP-AMP signalling protects bacteria against viral infection. Nature. 2019;574(7780):691-5. Epub 20190918. doi: 10.1038/s41586-019-1605-5. PubMed PMID: 31533127.
19. Morehouse BR, Govande AA, Millman A, Keszei AFA, Lowey B, Ofir G, et al. STING cyclic dinucleotide sensing originated in bacteria. Nature. 2020;586(7829):429-33. Epub

20200902. doi: 10.1038/s41586-020-2719-5. PubMed PMID: 32877915; PubMed Central PMCID: PMC7572726.
20. Pinilla-Redondo R, Shehreen S, Marino ND, Fagerlund RD, Brown CM, Sørensen SJ, et al. Discovery of multiple anti-CRISPRs highlights anti-defense gene clustering in mobile genetic elements. Nat Commun. 2020;11(1):5652. Epub 20201106. doi: 10.1038/s41467-020-19415-3. PubMed PMID: 33159058; PubMed Central PMCID: PMC7648647.
21. Gross M, Marianovsky I, Glaser G. MazG -- a regulator of programmed cell death in Escherichia coli. Mol Microbiol. 2006;59(2):590-601. doi: 10.1111/j.1365-2958.2005.04956.x. PubMed PMID: 16390452.
22. Engelberg-Kulka H, Hazan R, Amitai S. mazEF: a chromosomal toxin-antitoxin module that triggers programmed cell death in bacteria. J Cell Sci. 2005;118(Pt 19):4327-32. doi: 10.1242/jcs.02619. PubMed PMID: 16179604.
23. Culviner PH, Laub MT. Global Analysis of the E. coli Toxin MazF Reveals Widespread Cleavage of mRNA and the Inhibition of rRNA Maturation and Ribosome Biogenesis. Mol Cell. 2018;70(5):868-80.e10. Epub 20180531. doi: 10.1016/j.molcel.2018.04.026. PubMed PMID: 29861158; PubMed Central PMCID: PMC8317213.
24. Varik V, Oliveira SRA, Hauryliuk V, Tenson T. HPLC-based quantification of bacterial housekeeping nucleotides and alarmone messengers ppGpp and pppGpp. Sci Rep. 2017;7(1):11022. Epub 20170908. doi: 10.1038/s41598-017-10988-6. PubMed PMID: 28887466; PubMed Central PMCID: PMC5591245.
25. Kriel A, Bittner AN, Kim SH, Liu K, Tehranchi AK, Zou WY, et al. Direct regulation of GTP homeostasis by (p)ppGpp: a critical component of viability and stress resistance. Mol Cell. 2012;48(2):231-41. Epub 20120913. doi: 10.1016/j.molcel.2012.08.009. PubMed PMID: 22981860; PubMed Central PMCID: PMC3483369.
26. Sun Z, Wu R, Zhao B, Zeinert R, Chien P, You M. Live-Cell Imaging of Guanosine Tetra- and Pentaphosphate (p)ppGpp with RNA-based Fluorescent Sensors*. Angew Chem Int Ed Engl. 2021;60(45):24070-4. Epub 20211005. doi: 10.1002/anie.202111170. PubMed PMID: 34487413; PubMed Central PMCID: PMC8545912.
27. Engelberg-Kulka H, Reches M, Narasimhan S, Schoulaker-Schwarz R, Klemes Y, Aizenman E, et al. rexB of bacteriophage lambda is an anti-cell death gene. Proc Natl Acad Sci U S A. 1998;95(26):15481-6. doi: 10.1073/pnas.95.26.15481. PubMed PMID: 9860994; PubMed Central PMCID: PMC28068.
28. Gao L, Altae-Tran H, Böhning F, Makarova KS, Segel M, Schmid-Burgk JL, et al. Diverse enzymatic activities mediate antiviral immunity in prokaryotes. Science.

2020;369(6507):1077-84. doi: 10.1126/science.aba0372. PubMed PMID: 32855333; PubMed Central PMCID: PMC7985843.
29. Pedersen LC, Benning MM, Holden HM. Structural investigation of the antibiotic and ATP-binding sites in kanamycin nucleotidyltransferase. Biochemistry. 1995;34(41):13305-11. doi: 10.1021/bi00041a005. PubMed PMID: 7577914.
30. Duncan-Lowey B, McNamara-Bordewick NK, Tal N, Sorek R, Kranzusch PJ. Effector-mediated membrane disruption controls cell death in CBASS antiphage defense. Mol Cell. 2021;81(24):5039-51.e5. Epub 20211115. doi: 10.1016/j.molcel.2021.10.020. PubMed PMID: 34784509.
31. Essuman K, Summers DW, Sasaki Y, Mao X, Yim AKY, DiAntonio A, et al. TIR Domain Proteins Are an Ancient Family of NAD. Curr Biol. 2018;28(3):421-30.e4. Epub 20180125. doi: 10.1016/j.cub.2017.12.024. PubMed PMID: 29395922; PubMed Central PMCID: PMC5802418.
32. Essuman K, Summers DW, Sasaki Y, Mao X, DiAntonio A, Milbrandt J. The SARM1 Toll/Interleukin-1 Receptor Domain Possesses Intrinsic NAD. Neuron. 2017;93(6):1334-43.e5. doi: 10.1016/j.neuron.2017.02.022. PubMed PMID: 28334607; PubMed Central PMCID: PMC6284238.
33. Tamura K, Stecher G, Kumar S. MEGA11: Molecular Evolutionary Genetics Analysis Version 11. Mol Biol Evol. 2021;38(7):3022-7. doi: 10.1093/molbev/msab120. PubMed PMID: 33892491; PubMed Central PMCID: PMC8233496.
34. Jones DT, Taylor WR, Thornton JM. The rapid generation of mutation data matrices from protein sequences. Comput Appl Biosci. 1992;8(3):275-82. doi: 10.1093/bioinformatics/8.3.275. PubMed PMID: 1633570.
35. Crooks GE, Hon G, Chandonia JM, Brenner SE. WebLogo: a sequence logo generator. Genome Res. 2004;14(6):1188-90. doi: 10.1101/gr.849004. PubMed PMID: 15173120; PubMed Central PMCID: PMC419797.
36. Waterhouse AM, Procter JB, Martin DM, Clamp M, Barton GJ. Jalview Version 2--a multiple sequence alignment editor and analysis workbench. Bioinformatics. 2009;25(9):1189-91. Epub 20090116. doi: 10.1093/bioinformatics/btp033. PubMed PMID: 19151095; PubMed Central PMCID: PMC2672624.
37. Saha CK, Sanches Pires R, Brolin H, Delannoy M, Atkinson GC. FlaGs and webFlaGs: discovering novel biology through the analysis of gene neighbourhood conservation. Bioinformatics. 2021;37(9):1312-4. doi: 10.1093/bioinformatics/btaa788. PubMed PMID: 32956448; PubMed Central PMCID: PMC8189683.

38. Hauser M, Steinegger M, Söding J. MMseqs software suite for fast and deep clustering and searching of large protein sequence sets. Bioinformatics. 2016;32(9):1323-30. Epub 20160106. doi: 10.1093/bioinformatics/btw006. PubMed PMID: 26743509.
39. Mirdita M, Steinegger M, Söding J. MMseqs2 desktop and local web server app for fast, interactive sequence searches. Bioinformatics. 2019;35(16):2856-8. doi: 10.1093/bioinformatics/bty1057. PubMed PMID: 30615063; PubMed Central PMCID: PMC6691333.

Figure 1. Phage nucleotidytransferases synthesize CDN products.

(A) Dendrogram of phage NTases, MNT, and KNT clades within the DNA polymerase-β superfamily, built using alignment of protein sequences. Open and filled purple circles respectively indicate Av05 and BCP1 phage NTases analyzed in this study.

(B) Sequence LOGO diagram showing divergence of NTase sequences across two sites. Red asterisk indicates major catalytic site.

(C) Overlaid MALDI-MS chromatograms showing products generated by wild-type and mutant BCP1 phage NTase. Major products with masses corresponding to 3'3'cGAMP and cAA are shown. Inset shows chromatogram for wild-type BCP1 NTase across a wider m/z range. Results are representative of n=3 experiments.

(D) MALDI-MS chromatogram showing reaction products generated by Av05 phage NTase. Results are representative of n=2 experiments.

See also Figure S1.

Figure 2. Phage nucleotidyltransferases impair the activity of a TIR-STING death effector.

(A) NAD+ hydrolysis assay. *S. falciparum* (*Sf*) TIR-STING NAD+ cleavage activity was measured using the fluorescent substrate ε-NAD, in the absence or presence of increasing amounts of wild-type or catalytically inactive forms of BCP1 and Av05 phage NTases across a 10-fold range in concentration. Graphs show mean values with s.d. from n=4 experiments.

(B) CFU assay showing relative viability of *E. coli* transformed with the indicated combinations of *Sf*TIR-STING and the wild-type or catalytic mutant forms of BCP1 or Av05 NTase, or vector control. Results are representative of n=3 experiments.

See also Figure S2.

Figure 3. Functional screening identifies Acs1, a phage MazG-like protein that confers protection against TIR-STING toxicity.

(A) Examples of phage genomic loci containing NTases in close proximity to anti-restriction DNA methyltransferases and NAD biosynthetic enzymes.

(B) Schematic of plasmid-based functional screen. A plasmid library of phage genes selected on the basis of genomic proximity to NTase-encoding genes was transformed into *E. coli* hosts together with empty vector (EV) or inducible TIR-STING plasmid. Culture samples were withdrawn immediately prior to induction or following overnight growth. The relative representation of genes within the phage library for each strain and at each time point was then determined by deep sequencing.

(C) Volcano plot showing mean enrichment of phage genes in host cells co-expressing TIR-STING, normalized to EV controls. Phage genes significantly enriched ($P < 0.05$) in hosts co-expressing TIR-STING are displayed in purple. Acs1 is indicated with an orange outline.

(D) Top, schematic representation of Acs1 and MaxG proteins. The twin catalytic motifs are denoted by red asterisks. Bottom, multiple sequence alignment of phage and bacteria MazG family members. Conserved catalytic residues are highlighted in blue.

(E) Pyrophosphatase assay measuring activity of Acs1 on ppGpp and GTP substrates across a range of concentrations. The shaded area shows the 95% confidence interval of the Km of Acs1 for ppGpp. Results from two independent replicate experiments are plotted for each substrate.

See also Figure S3.

Figure 4. Acs1 depletes the starvation alarmones (p)ppGpp.

(A) Visualization of cellular (p)ppGpp levels using RNA-based fluorescent sensor (green) and cytosolic RFP (red) in live bacteria grown in media containing glucose, or following treatment with the glycolysis inhibitor α-MG to induce starvation, or following induction of TIR-STING or control vector. Scale bar, 50 μm. Results are representative of n=3 experiments.

(B) Violin plot of (p)ppGpp sensor signal intensities in live cells grown in glucose, treated with the chemical starvation agent α-MG, or following induction of TIR-STING. Dashed lines indicate quartiles.

(C) Cellular (p)ppGpp sensor (green) and cytosolic RFP fluorescence (red) in cells grown in complete media containing glucose, or following starvation induced by α-MG in the absence or presence of Acs1. Scale bar, 50 μm. Results are representative of n=3 experiments.

(D) Violin plot of (p)ppGpp sensor signal intensities in live cells following treatment with α-MG, in the presence of Acs1 or empty control vector. Dashed lines indicate quartiles.

Figure 5. Function of RelA and the MazEF toxin-antitoxin in TIR-dependent abortive infection.

(A) CFU assays showing effects of genetic inactivation of *mazG*, *relA* or *mazEF*, or expression of RexB or Acs1, on TIR-STING cytotoxicity. Results are representative of n=4 replicate experiments.

(B) Quantification of CFU assay results. Bar graphs show mean values, error bars show s.d. from n=4 experiments.

(C) Phage plaque formation assay. Bacterial lawns grown from *E. coli* expressing a retron-TIR defense system or carrying an empty vector control, each in the absence or presence of Acs1, were infected with droplets containing 10-fold serial dilutions of T5 phage. Results are representative of n=3 replicate experiments.

(D) Model depicting suppression of host immunity by phage NTases and Acs1, which intercede at distinct points in abortive infection suicide responses orchestrated by immune effectors containing TIR and STING domains.

Figure 1

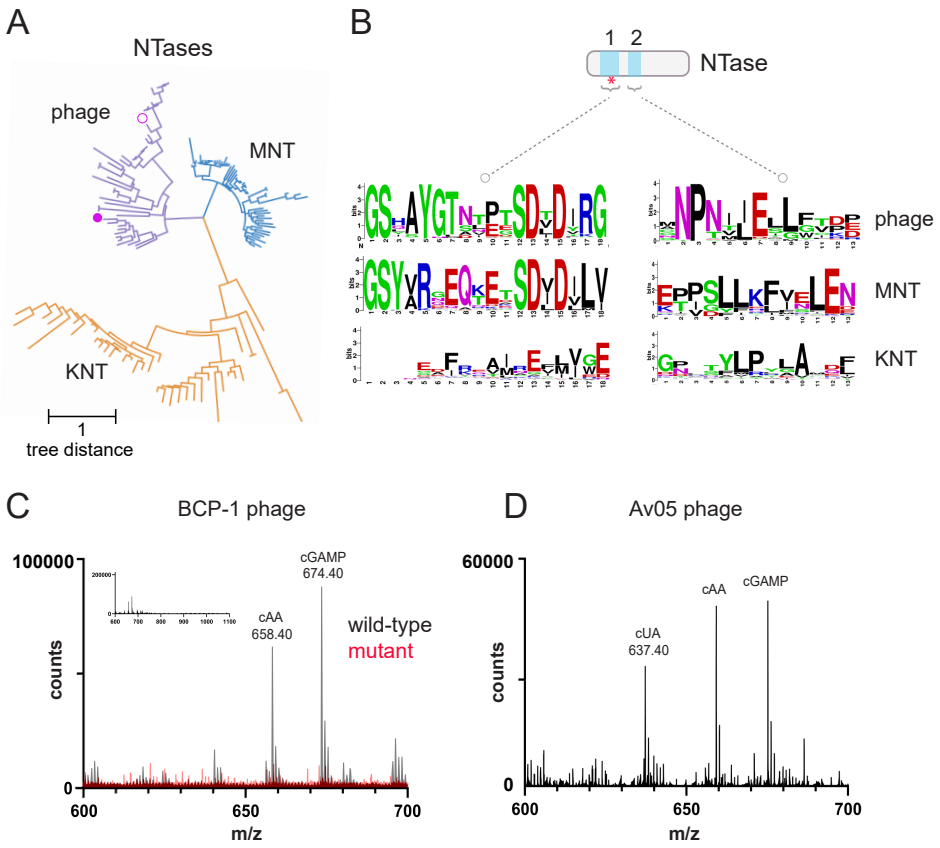
A
NTases
phage
MNT
KNT
1
tree distance
B
1 2
NTase
phage
MNT
KNT
C
BCP-1 phage
100000
counts
0
600
650
700
m/z
cGAMP
674.40
cAA
658.40
wild-type
mutant
D
Av05 phage
60000
counts
0
600
650
700
m/z
cUA
637.40
cAA
cGAMP

Figure 2

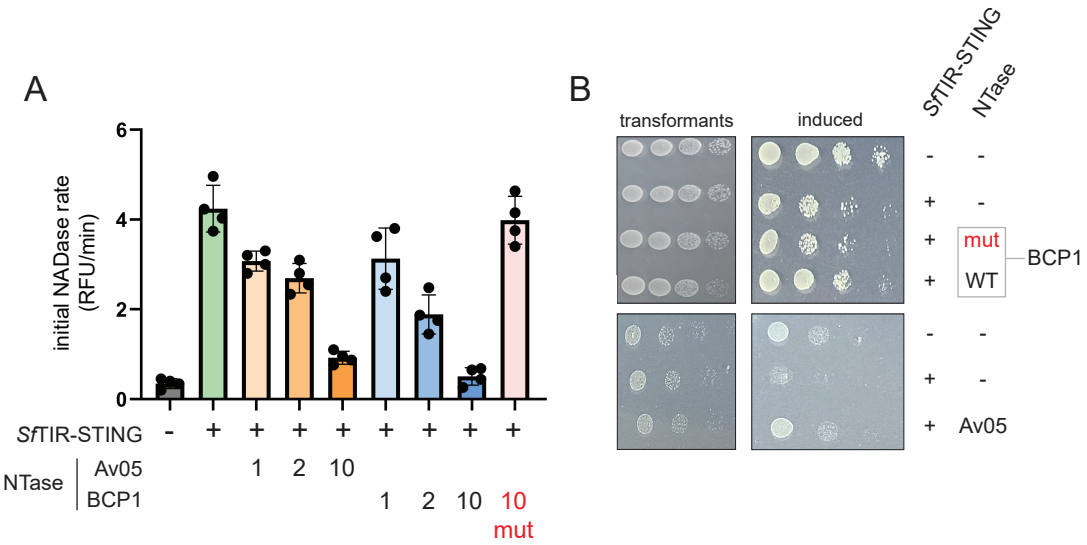
A
initial NADase rate (RFU/min)
6
4
2
0
SfTIR-STING - + + + + + + + +
NTase
Av05 1 2 10
BCP1 1 2 10 10 mut
B
transformants
induced
SfTIR-STING
NTase
- -
+ -
+ mut
+ WT
BCP1
- -
+ -
+ Av05

Figure 3

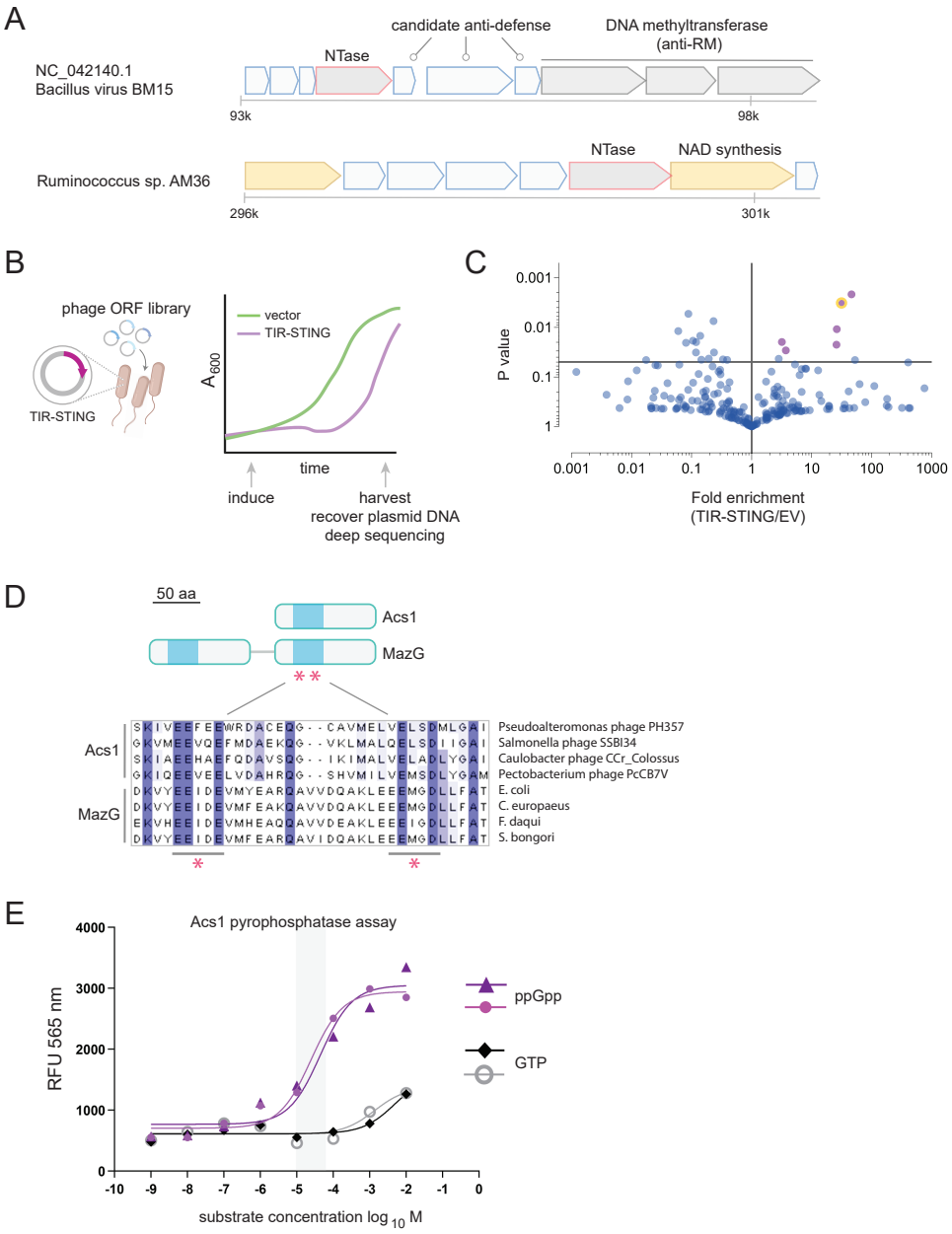
A
candidate anti-defense
DNA methyltransferase
(anti-RM)
NTase
NC_042140.1
Bacillus virus BM15
93k
98k
NTase
NAD synthesis
Ruminococcus sp. AM36
296k
301k
B
phage ORF library
TIR-STING
vector
TIR-STING
A600
time
induce
harvest
recover plasmid DNA
deep sequencing
C
P value
0.001
0.01
0.1
1
0.001
0.01
0.1
1
10
100
1000
Fold enrichment
(TIR-STING/EV)
D
50 aa
Acs1
MazG
Acs1
MazG
Pseudoalteromonas phage PH357
Salmonella phage SSBI34
Caulobacter phage CCr_Colossus
Pectobacterium phage PcCB7V
E. coli
C. europaeus
F. daqui
S. bongori
E
Acs1 pyrophosphatase assay
RFU 565 nm
4000
3000
2000
1000
0
-10
-9
-8
-7
-6
-5
-4
-3
-2
-1
0
substrate concentration log 10 M
ppGpp
GTP

Figure 4

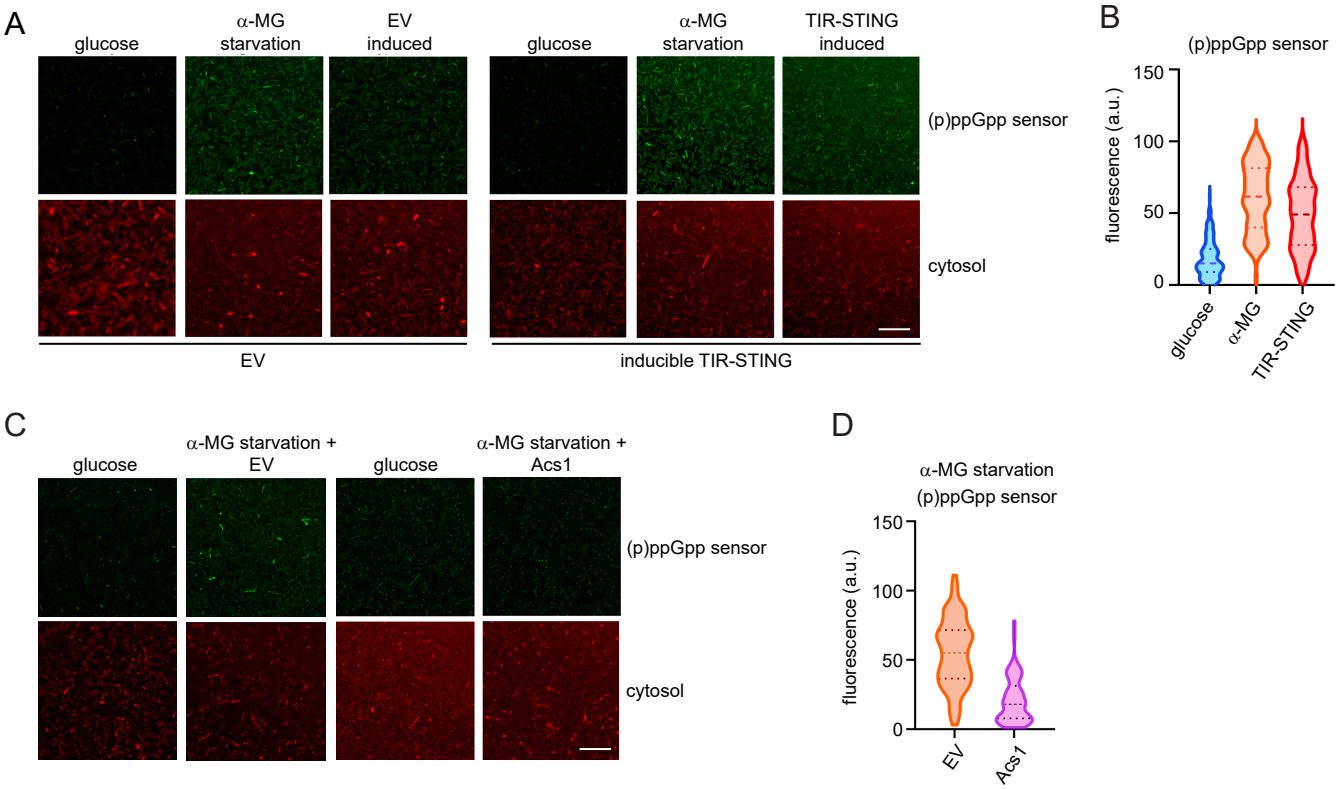
A
glucose
α-MG starvation
EV induced
glucose
α-MG starvation
TIR-STING induced
(p)ppGpp sensor
cytosol
EV
inducible TIR-STING
B
(p)ppGpp sensor
fluorescence (a.u.)
150
100
50
0
glucose
α-MG
TIR-STING
C
glucose
α-MG starvation + EV
glucose
α-MG starvation + Acs1
(p)ppGpp sensor
cytosol
D
α-MG starvation
(p)ppGpp sensor
fluorescence (a.u.)
150
100
50
0
EV
Acs1

Figure 5

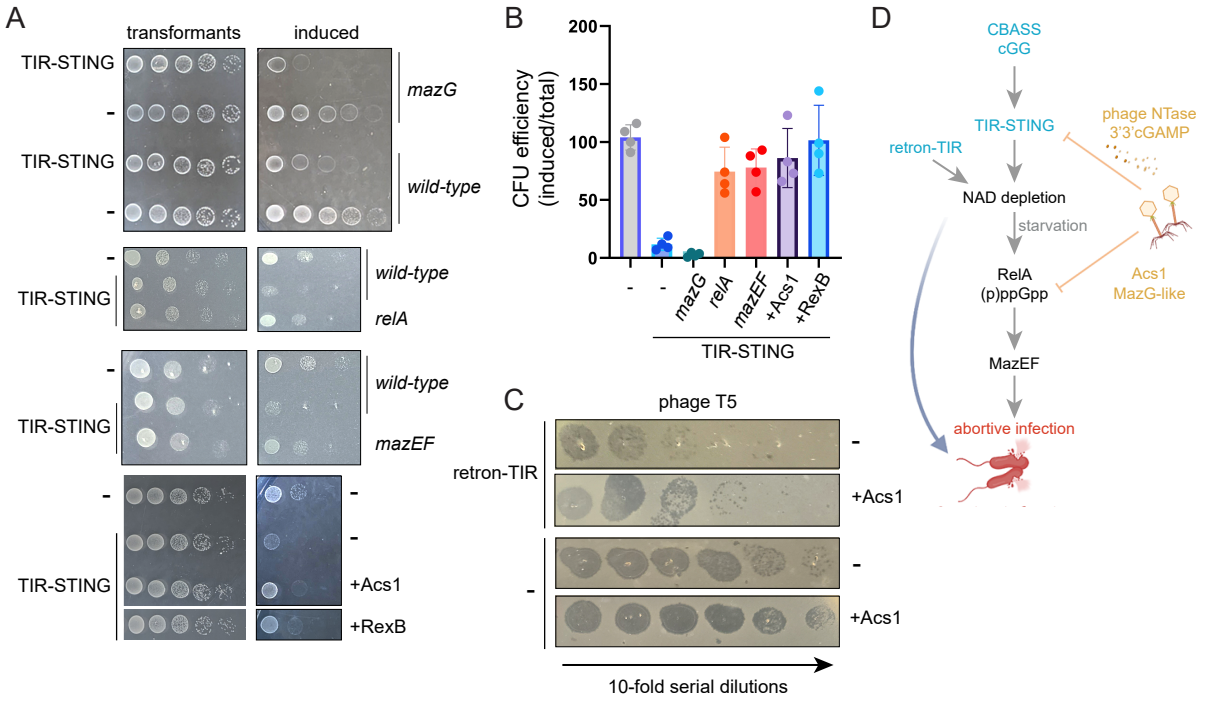
A
transformants
induced
TIR-STING
-
TIR-STING
-
mazG
wild-type
-
TIR-STING
wild-type
relA
-
TIR-STING
wild-type
mazEF
-
TIR-STING
-
-
+Acs1
+RexB
B
CFU efficiency (induced/total)
200
150
100
50
0
-
-
mazG
relA
mazEF
+Acs1
+RexB
TIR-STING
C
phage T5
retron-TIR
-
+Acs1
-
-
+Acs1
10-fold serial dilutions
D
CBASS
cGG
TIR-STING
phage NTase
3'3'cGAMP
retron-TIR
NAD depletion
starvation
RelA
(p)ppGpp
Acs1
MazG-like
MazEF
abortive infection